CARBON letters

Original Articles
Carbon Letters Vol. 20, 1-9 (2016)

Adsorption capability of activated carbon synthesized from coconut shell

Md Shariful Islam[1], Bee Chin Ang[1,♣], Samira Gharehkhani[2] and Amalina Binti Muhammad Afifi[1]

[1]Center of Advanced Materials, Department of Mechanical Engineering, University of Malaya, Kuala Lumpur 50603, Malaysia
[2]Department of Mechanical Engineering, University of Malaya, Kuala Lumpur 50603, Malaysia

Article Info
Received 2 December 2015
Accepted 18 July 2016

♣Corresponding Author
E-mail: amelynang@um.edu.my
Tel: +60-79675258

Open Access
DOI: http://dx.doi.org/10.5714/CL.2016.20.001

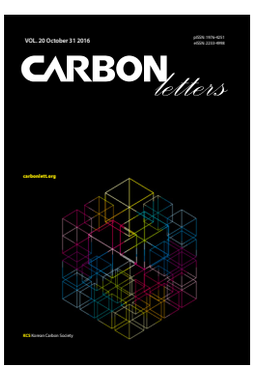

http://carbonlett.org

pISSN: 1976-4251
eISSN: 2233-4998

Abstract

Activated carbon was synthesized from coconut shells. The Brunauer, Emmett and Teller surface area of the synthesized activated carbon was found to be 1640 m^2/g with a pore volume of 1.032 cm^3/g. The average pore diameter of the activated carbon was found to be 2.52 nm. By applying the size-strain plot method to the X-ray diffraction data, the crystallite size and the crystal strain was determined to be 42.46 nm and 0.000489897, respectively, which indicate a perfect crystallite structure. The field emission scanning electron microscopy image showed the presence of well-developed pores on the surface of the activated carbon. The presence of important functional groups was shown by the Fourier transform infrared spectroscopy spectrum. The adsorption of methyl orange onto the activated carbon reached 100% after 12 min. Kinetic analysis indicated that the adsorption of methyl orange solution by the activated carbon followed a pseudo-second-order kinetic mechanism ($R^2 > 0.995$). Therefore, the results show that the produced activated carbon can be used as a proper adsorbent for dye containing effluents.

Key words: coconut shell, activated carbon, dye adsorption, size-strain plot, specific surface area

1. Introduction

In this era of industrialization, industries like textile (especially in the dyeing sector), leather, carpet, rubber, food processing, pharmaceutical, cosmetic, plastic, pulp and paper manufacturing use synthetic dyes regularly and discharge a large amount of dye containing water into the environment [1-4]. Nowadays, the annual production of commercial dyes is over 9 million tons with over one hundred thousand types of dyes [5,6]. It has been reported that about 10%–20% of dyes are discharged into water during the dyeing process [7]. Dyes usually contain recalcitrant molecules which are potentially carcinogenic, toxic and resistant to aerobic digestion and inhibit the reaction of oxidizing agents [8,9]. The very complex molecular structures of these dyes make them imperishable [10,11]. Even a small amount of dye can be harmful to both terrestrial and aquatic animals as well as humans [12]. Thus, these dyes require proper treatment before being discharged into the environment.

Among the physical, chemical and biological methods of dye removal, oxidation (using oxidizing agents like ozone, ultraviolet [UV] irradiation, and hydrogen peroxide), membrane separation, coagulation and flocculation, and adsorption are commonly used [3,13]. However, other than the adsorption techniques, these methods have either high costs and/or are technically complicated [14]. The adsorption method is highly preferable due to its low cost consumption, easy operation, higher efficiency, insensitivity to toxic materials and versatility [1,13,15-17].

The commonly used adsorbents are modified clays, waste materials, natural polymers and biopolymers (usually poly saccharides such as chitosan and its derivatives), zeolites,

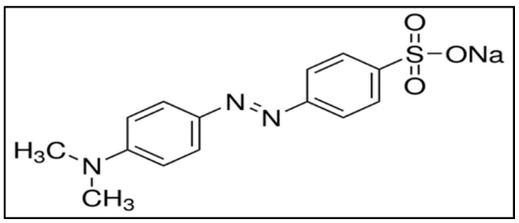

Fig. 1. Chemical structure of methyl orange.

activated carbon, etc. Other than activated carbon, the other adsorbents have some undesirable disadvantages in dye removal such as complex separation techniques from the adsorbate, little or no resistance against acid solutions, and poor mechanical strength and versatility. Additionally, these adsorbents need a long contact time with the adsorbate [18-22]. Therefore, with a high specific surface area, large pore volume, suitable pore size (2–50 nm), high degree of surface reactivity and effective adsorption quality, activated carbon has become the most desirable adsorbent [23-26].

Methyl orange is one of the most used anionic dyes, which belongs to the azo group of dyes, in textile manufacturing and paper and food processing industries. The presence of the azo group (-N=N) in the molecules of methyl orange and its low biodegradability make it a serious threat to the environment [27]. The chemical structure of methyl orange is shown in Fig. 1.

Many studies have been done on the removal of dye molecules from aqueous solutions by activated carbon; however, most of them were unable to remove dye molecules completely (100%) in a short time period [28-32]. Hesas et al. [28] reported the highest adsorption (94.6%) among all the studies. The reason for this could be due to the relatively smaller surface area of activated carbon because it is obvious that a higher surface area leads to a higher adsorption efficiency [33]. Therefore, the aim of this study was to synthesize activated carbon from coconut shells with a higher surface area to completely remove dye molecules from an aqueous solution within the shortest possible time.

In this study, activated carbon was synthesized from a coconut shell and then characterized. Additionally, the synthesized activated carbon in this study was verified as an effective adsorbent by the removal of methyl orange (sodium 4-[(4-dimethylamino) phenyldiazenyl] benzene sulfonate).

2. Experimental

2.1. Synthesis of the activated carbon

In this study, we used coconut shells to produce activated carbon and methyl orange for the adsorption test. The use of both were in compliance with the ethical standards of Malaysian government. A coconut shell was washed with distilled water to remove undesirable impurities and dried in an oven at 120°C for 24 h. The washed and dried coconut shell was carbonized at 450°C for 3 h at a heating rate of 10°C/min. under a flow of purified nitrogen. The carbonized sample was washed with distilled water and kept in an oven at 70°C for 48 h for complete drying. The dried char was mixed with potassium hydroxide (KOH) pellets in a 1:4 (KOH/char) impregnation ratio followed by the addition of 15 mL of distilled water to the mixture. Then, the mixture was stirred with a magnetic stirrer for 4 h. The activation step was done in a tube furnace at 400°C for 30 min and 600°C for 2 h with a heating rate of 5°C/min. under a purified nitrogen flow. The activated product was washed with deionized water and hydrochloric acid until the pH of the washing solution reached 6–7. Then, the activated carbon was kept in an oven for 24 h.

2.2. Characterization of the activated carbon

Synthesized activated carbon was analyzed with the N_2 adsorption desorption test based on the Brunauer-Emmett-Teller (BET) principle, X-ray diffraction (XRD), field emission scanning electron microscopy (FESEM) and Fourier transform infrared spectroscopy (FTIR).

2.2.1. Nitrogen adsorption isotherm analysis

The pore structure characteristics of the activated carbon were determined by nitrogen adsorption with a Sorptomatic 1990. During the experiment, the carbon was degassed at 120°C for 12 h in a vacuum condition. The BET surface area was determined with the standard BET equation applied in a relative pressure range from 0.06 to 0.3. The total pore volume was calculated at a relative pressure of approximately 0.985, and at this relative pressure, all pores were completely filled with nitrogen gas.

2.2.2. Crystallographic analysis

Powder XRD patterns were recorded using the PANalytical Empyrean X-ray diffractometer (EA Almelo, the Netherlands) with monochromated Cu Kα radiation (λ = 1.54056 A°) operated at 45 kV and 40 mA with a step size of 0.026° and a scanning rate of 0.1° s^{-1} over a 2θ range from 5° to 80°. The crystallite size of the produced sample was calculated with the following size-strain plot (SSP) equation [34].

$$(d_{hkl}\beta_{hkl}\cos\theta)^2 = \frac{K}{D}(d_{hkl}^2\beta_{hkl}\cos\theta) + \left(\frac{\varepsilon}{2}\right)^2 \quad (1)$$

Here, d_{hkl} represents the lattice distance between the (*hkl*) planes; β_{hkl} is the peak full width at half height (FWHM) in radians. K, D, ε and θ correspond to the constant $\left(\frac{4}{3}\right)$, crystallite size, lattice strain and half diffraction angle (radian). When $(d_{hkl}\beta_{hkl}\cos\theta)^2$ is plotted against $(d_{hkl}^2\beta_{hkl}\cos\theta)$ for the characteristics peaks of the activated carbon, the crystallite size is measured from the slope of the linearly fitted data and the strain from the root of the y-intercept.

2.2.3. Surface morphology analysis

FESEM (high-resolution FEI Quanta 200F; Hitachi, Tokyo, Japan) was used to observe the surface morphology of the activated carbon, and energy dispersive X-ray spectroscopy (EDS) analysis was done to determine the elements in the sample. The average composition was obtained by taking the average of 4 points.

2.2.4. FTIR analysis

Nicolet iS10 FTIR spectrometer from Thermo Scientific with a spectral range from 4000 to 400 cm^{-1} was used to determine the functional groups of the activated carbon.

2.3. Adsorption test

In the adsorption test, 0.2 g of activated carbon were added to 0.02 L of methyl orange solution (30 mg/L) and agitated gently with a magnetic stirrer for 12 min to examine the adsorption behavior of the activated carbon. The sample was collected at different time intervals, and the dye concentration (C_t) was calculated with the Varian CARY 50 probe type UV-vis spectrophotometer (Agilent Technologies Inc., Santa Clara, CA, USA). The amount of dye adsorbed (q_t) onto the activated carbon was calculated with the following formula [35,36]:

$$q_t = \frac{c_0 - c_t}{m} V \quad (2)$$

here, C_0 and C_t represent, respectively, the initial and equilibrium concentrations of methyl orange solution in (mg L^{-1}), and V is the volume of the solution in liters, and m is the weight of the activated carbon used in grams.

The percentage removal of methyl orange was calculated with the following equation [37]:

$$Removal(\%) = \frac{c_0 - c_t}{c_0} \times 100 \quad (3)$$

3. Results and Discussion

3.1. Nitrogen adsorption-desorption isotherm of the synthesized activated carbon

The adsorption capacity of an adsorbent largely depends on the number of pores and the size of the surface area. Porosity in carbon is developed through an activation process by creating a more orderly porous structure [38]. There are usually four stages in pore development during the activation process: 1) opening of previously inaccessibly pores; 2) creation of new pores by selective activation; 3) widening of existing pores; and 4) merging of existing pores due to pore wall breakage [39]. Fig. 2 shows the nitrogen adsorption-desorption isotherm of the activated carbon prepared by KOH activation.

Fig. 2a shows that the adsorption-desorption isotherm of the activated carbon is for a Type IV isotherm based on the International Union of Pure and Applied Chemistry (IUPAC) classification [40]. A characteristic feature of Type IV isotherms is that they possess a hysteresis loop which is associated with capillary condensation taking place in the mesopores which limits uptake at high relative pressures. From Fig. 2b, it is clear that the pore size ranges between 2 and 20 nm which proves the mesoporosity of the particle. The average pore diameter can be calculated with the following equation [41]:

$$D = \frac{4V}{A} \quad (4)$$

here, V and A denote the pore volume and specific surface area measured by the BET method. Therefore, the specific surface area and pore volume of the activated carbon were found to be 1640 m^2/g and 1.032 cm^3/g, respectively. The average pore diameter was found to be 2.52 nm.

3.2. Crystallographic analysis of the activated carbon

The synthesized activated carbon can be crystallographically characterized with XRD. Fig. 3 shows the X-ray diffractograms of the activated carbon before and after the activation process. Fig. 3a shows that the carbonized sample has five major peaks at 25.84, 42.4, 43.4, 49.5, and 79.25° (2θ). These peaks are also found in the final activated carbon sample.

The amorphous peak detected at around 26° (2θ) is assigned to the reflection from the (002) plane. The peaks at 42° and 79° (2θ) are assigned to the overlapped reflection from the (100), (101) and (110) plane, respectively [42]. The diffraction peaks at 2θ = 26 and 42 signify that both samples are composed of a carbonaceous material [43].

Peaks corresponding to potassium metal and potassium oxides usually appear at 42° and 49° (2θ) with 42° (2θ) denoting the "K" metal and 49° (2θ) the K_2CO_3 compound. The intensity of these peaks is increased in the sample after the activation process (Fig. 3b) compared to the sample before activation (Fig. 3a). The reason for this may be due to the overlapping of the peaks for K with the peaks for the (100), (101) plane of carbonaceous materials. A gasification reaction occurred during the KOH activation process in which KOH was converted to either K metal or K_2CO_3 [44]. Potassium metal remains in the final

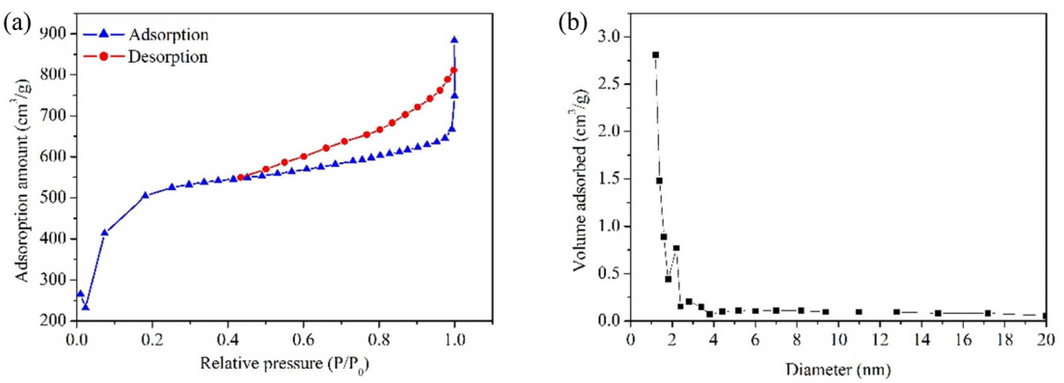

Fig. 2. (a) N_2 adsorption-desorption isotherms and (b) pore size distribution curve based on the Brunauer-Emmett-Teller method for the activated carbon.

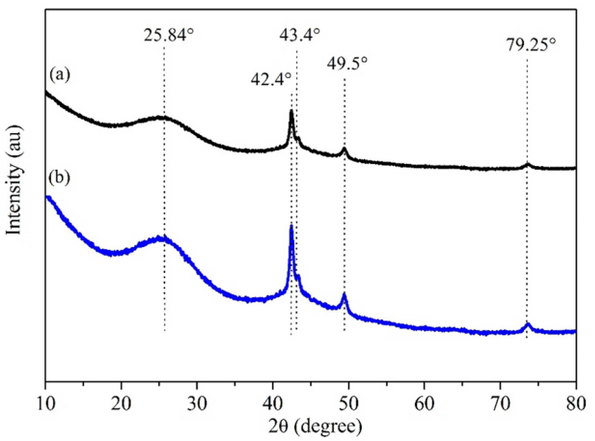

Fig. 3. X-ray diffraction patterns (a) carbonized sample and (b) activated carbon sample.

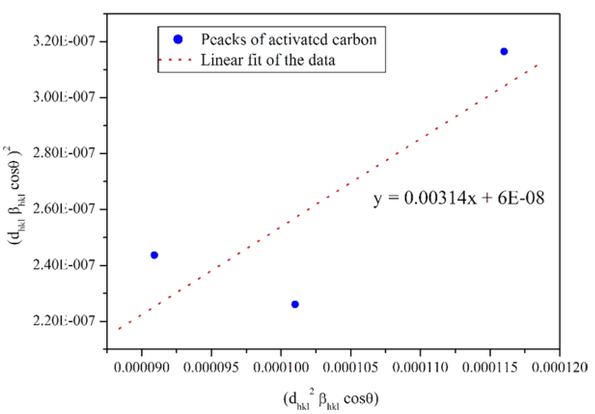

Fig. 4. The size-strain plot plot of the activated carbon.

activated carbon because the boiling point of K is 780°C [45]. However, 600°C was the highest temperature used during the activation process in this study.

The presence of the (100) and (110) plane indicates that the produced activated carbon is composed of small domains of ordered graphene sheets which shows the regularity of the crystal structure [46]. Liu and Watanasiri [47] calculated the theoretical (002) Bragg peaks for powder samples to determine whether the sample is made of randomly oriented single layers, bilayers and trilayers as well as mixtures of randomly oriented bilayers. And according to Liu's result, synthesized activated carbon consists of randomly oriented single and multi-layer domains.

The FWHM of the four crystalline peaks at 42.3916°, 43.4253°, 49.4610° and 79.2510° (2θ) found in the activated carbon sample (Fig. 3b) were used to calculate the crystallite size of the activated carbon. By applying the SSP method to the XRD data (as described in section 2.2.2), the crystallite size (D) was found to be 42.46 nm, and the corresponding crystal strain (ε) was equal to 0.000489897. The SSP is shown in Fig. 4. The crystallite size and crystal strain values show that the synthesized activated carbon has a perfect crystalline structure with no lattice displacement.

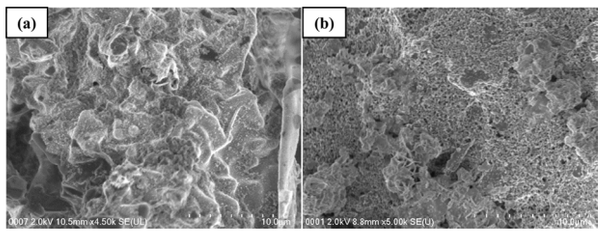

Fig. 5. Field emission scanning electron microscopy micrographs of the activated carbon (a) before activation and (b) after activation.

Table 1. Composition of the activated carbon

	Carbon (C) (%)	Oxygen (O) (%)	Nitrogen (N) (%)	Silicone (Si) (%)
Spot 1	76.7	20.5	2.6	0.2
Spot 2	78.9	18.5	2.3	0.3
Spot 3	79.1	17.9	2.8	0.2
Spot 4	83.5	13.6	2.7	0.2
Average	79.55	17.625	2.6	0.225

3.3. Surface morphology of the activated carbon

Fig. 5 shows the microstructure of the activated carbon before and after the activation process. It can be seen from Fig. 5a that before the carbonization process, a much smaller number of pores was present on the external surface of the activated carbon. However, after the activation process, well-developed pores are clearly visible on the surface of the activated carbon. This is in agreement with the 1.032 cm^3/g pore volume found by the BET surface analysis. These pores might be due to the evaporation of the chemical reagent (KOH) used during the carbonization process leaving behind the porous surface of the activated carbon [38].

The average compositions of the activated carbon are summarized in Table 1 which were acquired by the EDS analysis. Of note is that the activated carbon sample has a high carbon content. The presence of oxygen is mainly due to inadequate washing of the material. The presence of nitrogen may be due to the nitrogen gas flow during the carbonization and activation process. And the very low amount of silicone indicates the presence of a small amount of impurities. Thus, it can be concluded that carbon is the predominant component in the sample which indicates the carbonaceous nature of the sample.

3.4. FTIR analysis

The FTIR spectrum of the activated carbon is shown in Fig. 6. The broad band at 3346 cm^{-1} is related to the valence vibration of the hydrogen bonded O-H groups [48]. The reason for the occurrence of this band can be assigned to the O-H stretching mode of the hexagonal groups and adsorbed water. Additionally, the presence of strong hydrogen bonds is indicated by the

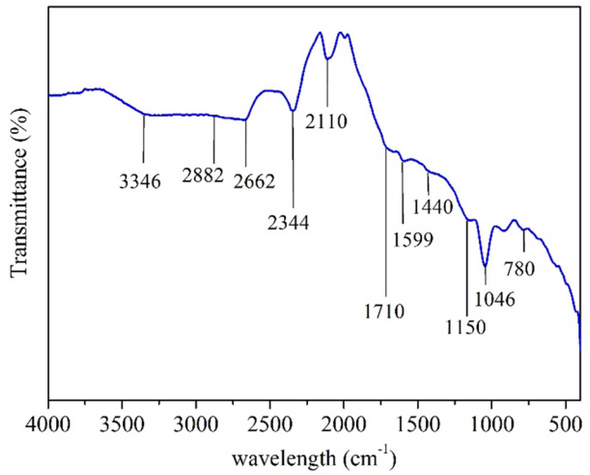

Fig. 6. Fourier transform infrared spectroscopy spectrum of the activated carbon synthesized from a coconut shell.

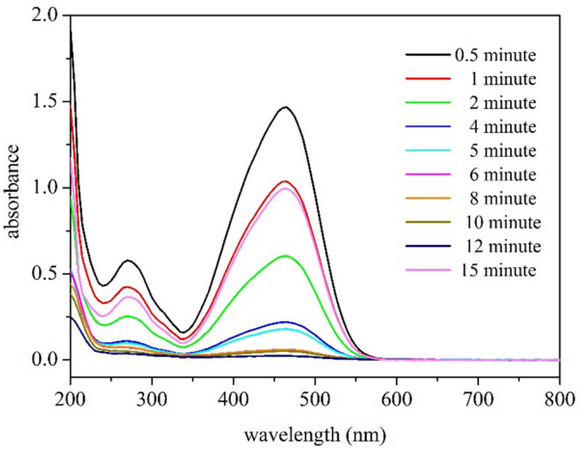

Fig. 7. Ultraviolet visible spectra of the methyl orange solution with different contact times with the activated carbon.

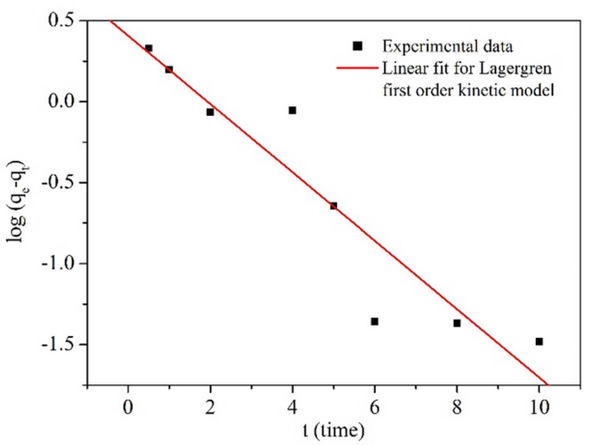

Fig. 8. Linear regression of the Lagergren first order kinetic model for the adsorption of methyl orange at room temperature.

position and asymmetry of this band at lower wave numbers [49]. The shoulder band at 2882 cm^{-1} may originate from the C-H stretching in the (-CH_2) and (-CH_3) groups [50,51]. The relatively wide band at 2344 cm^{-1} may either correspond to the symmetric (NH_3^+) stretching frequency [52] or to the carbon-oxygen bonds in the ketene groups [50]. Another relatively broad peak at ~2100 cm^{-1} is attributed to the allene (C=C=C) group [53]. A very small peak near 1700 cm^{-1} is assigned to the C=O stretching vibrations of ketones, aldehydes, lactones or carboxyl groups. The weak intensity of this peak indicates that this sample contains a small amount of carboxyl groups [53]. The band at 1599 cm^{-1} indicates the presence of (C–H, –C=C– and aromatic C=C) groups [54]. Moreover, the band at 1440 cm^{-1} may correspond to the O-H bending band. In the region (1400–1600) cm^{-1}, there are clusters of complex bands, which may be due to the presence of aromatic (C=C) bands and various substitution modes of the aromatic rings [55]. The broad band at 1150 cm^{-1} has been assigned to C-O single bonds such as those in ethers, phenols, acids and esters [50,51].

The sharp peak at 1046 cm^{-1} represents the alcoholic C-O stretching vibration [55]. Bands below 950 cm^{-1} correspond to the out-of-plane deformation vibrations of the C-H groups in the aromatic structure [49,56]. In this region, the bands at 590 cm^{-1} and 675 cm^{-1} generally correspond to the stretch of the S=O and S-O group, and 670 cm^{-1} represents physisorbed carbon dioxide [57]. Other peaks detected in this region at 780 cm^{-1}, 652 cm^{-1} and 608 cm^{-1}, respectively, are assigned to the C-H out-of-plane bending in benzene derivatives, O–H stretching and C–O–H twist. The C–H out-of-plane bending in benzene derivatives has been commonly found on the surface of various activated carbons [58,59]. There are no peaks for SiO_2 at 1101, 944 and 470 cm^{-1}, which indicate that the synthesized activated carbon consists of no or very few SiO_2 [60]. This result is also shown by the EDS analysis in this study. Additionally, the FTIR spectra found here are in accordance with the results reported by Jung et al. [61] on a commercial granular activated carbon.

3.5. Adsorption of methyl orange by the synthesized activated carbon

The UV-vis spectra of methyl orange solution in contact with activated carbon is shown in Fig. 7. It can be seen from Fig. 7 that the characteristic peaks of benzene and the azo linkage of the methyl orange were found in the initial UV-vis spectra of the methyl orange at a wavelength of 270 and 464.9 nm, respectively. Therefore, it was observed that the intensity was reduced with an increase in the contact time. After 12 min, methyl orange removal reached 100%.

In order to predict the adsorption behavior of the activated carbon, Lagergren-first-order [62], pseudo-second-order [63] and Weber and Morris intra-particle diffusion reaction models [64] were used to determine the kinetics of the adsorption of methyl orange from an aqueous solution.

Lagergren first order kinetic model; the linear form of the Lagergren first order kinetic model is represented by the following formula.

Table 2. Kinetic parameters for the adsorption of methyl orange on the activated carbon

Kinetic model	Concentration (mg L^{-1})	q_e (exp., mg g^{-1})	q_e (cal, mg g^{-1})	Rate constant	R^2	SD (%)	C (mg g^{-1})
Lagergren first order kinetic model			2.56	0.486 min^{-1}	0.8868	27.493	NA
Pseudo second order kinetic model	30	3	3.14	0.2266 g mg^{-1} min^{-1}	0.9959	6.768	NA
Intra particle diffusion kinetic model			NA	0.86 mg g^{-1} min^{-1}	0.8632	32.361	0.63952

q_e, equilibrium adsorption capacity ; SD, standard deviation.

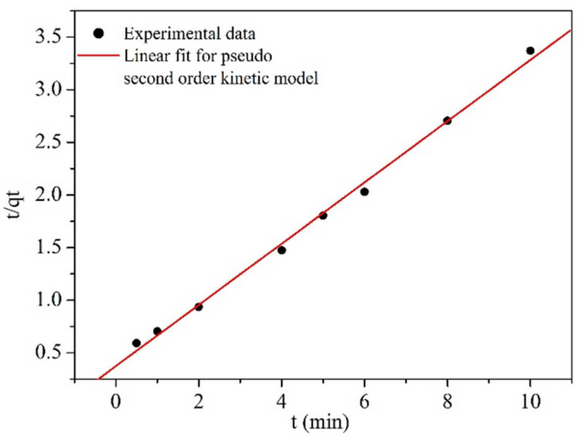

Fig. 9. Linear regression of the pseudo second order kinetic model for the adsorption of methyl orange at room temperature.

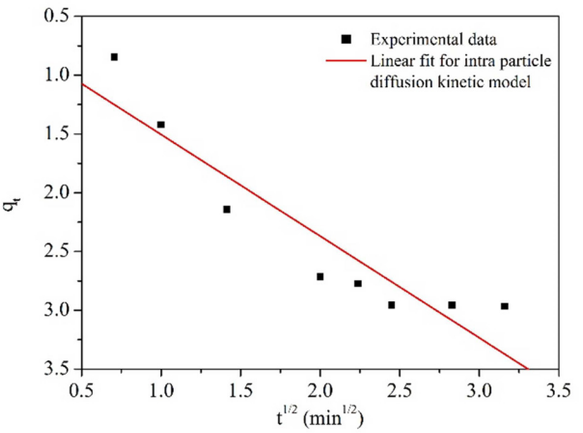

Fig. 10. Linear regression of the intra particle diffusion kinetic model for the adsorption of methyl orange at room temperature.

$$\log(q_e - q_t) = \log q_e - \frac{k_1 t}{2.303} \quad (5)$$

, where q_e and q_t represent the amounts of methyl orange adsorbed (mg/g) at equilibrium and at time t, respectively. k_1 (min^{-1}) is the Lagergren rate constant. Fig. 8 shows the plots of $\log(q_e - q_t)$ versus t of the Lagergren first order kinetic model. Values for q_e and k_1 at different initial concentrations were calculated, respectively, from the slope and intercept. These are presented in Table 2.

The pseudo-second-order kinetic model; the linear form of the pseudo-second-order kinetic model is represented by the following formula.

$$\frac{t}{q_t} = \frac{1}{k_2 q_e^2} + \frac{t}{q_e} \quad (6)$$

, where q_e and q_t represent the amounts of methyl orange adsorbed (mg/g) at equilibrium and at time t, respectively. The rate constant of the pseudo second order adsorption model is represented by K_2 in (g/mg/min.). Fig. 9 shows the plots of t/q_t versus t. Values for K_2 and q_e were calculated, respectively, from the slope and intercept point of the graph. These values are presented in Table 2.

Weber and Morris intra-particle diffusion reaction model; the linear form of the intra-particle diffusion reaction model is represented by the following formula.

$$q_t = k_{id} t^{\frac{1}{2}} + c \quad (7)$$

, where c is the intercept which reflects the boundary layer effect; q_e and q_t represent the amounts of methyl orange adsorbed (mg/g) at equilibrium and at time t, respectively, and k_{id} is the intra particle diffusion reaction model. Fig. 10 shows the plot of q_t versus $t^{1/2}$. The values for K_{id} and c were calculated, respectively, from the slope and intercept and are presented in Table 2.

Of note in Table 2 is that there is a notable difference between the theoretical value of q_e (2.56 mg g^{-1}) determined from the Lagergren first order kinetic model and the experimental value. Moreover, the correlation coefficient (R^2 = 0.7201) is significantly low. Therefore, the adsorption kinetics of methyl orange cannot be explained by this model. On the other hand, it is obvious from Table 2 that the adsorption kinetics of methyl orange on the activated carbon can be better interpreted by the pseudo-second-order kinetic model because it has a high correlation coefficient ($R^2 > 0.99$). Moreover, the theoretical value of q_e (3.14 mg g^{-1}) is the closest to the experimental data (3 mg g^{-1}). Hence, it can be concluded that the rate of direct adsorption controls the overall sorption kinetics. Additionally, according to Blanchard et al. [65], it can be assumed that the rate of the ion exchange reaction occurring on the surface between the adsorbent and adsorbate is responsible for the removal kinetics.

From the analysis of the intraparticle diffusion model, the value of C was found to be 0.63952 mg g^{-1} which indicates that there is less contribution from intraparticle diffusion on the adsorption kinetics of methyl orange on the activated carbon. If the value of C is equal to zero, then it can be assumed that the

adsorption was solely governed by intraparticle diffusion. It is found that the plots of q_t versus $t^{1/2}$ do not pass through the origin but intercept at the Y-axis which signifies that intraparticle diffusion as a rate limiting step is not only responsible but also some boundary layer effect as well.

4. Conclusions

In this study, activated carbon was successfully synthesized from a coconut shell with the potassium hydroxide activation process. This activated carbon was characterized by BET, XRD, FESEM and FTIR. A comprehensive study was performed on its adsorption efficiency for the removal of methyl orange from an aqueous solution.

BET surface analysis revealed that the synthesized sample is a mesoporous solid. XRD analysis proved that the sample had a perfect crystallite structure, and the FESEM images showed the presence of well-developed pores on the surface of the activated carbon sample.

A kinetic study showed that the adsorption behavior of the activated carbon followed the pseudo-second-order kinetic model. In addition, the experimental result showed that 100% dye removal was obtained by the adsorption process in 12 min.

Conflict of Interest

No potential conflict of interest relevant to this article was reported.

Acknowledgements

The authors greatly appreciate the financial support from the University of Malaya under a University of Malaya Research Grant (UMRG) (Grant No. RP022C-13AET), Fundamental Research Graduate Scheme (FRGS) (Grant No. FP026-2014B) and Postgraduate Research Fund (PPP) (Grant No. PG150-2015A).

References

[1] Dong Y, Lin H, Qu F. Synthesis of ferromagnetic ordered mesoporous carbons for bulky dye molecules adsorption. Chem Eng J, **193-194**, 169, (2012). http://doi.org/10.1016/j.cej.2012.04.024.

[2] Zhao D, Zhang W, Chen C, Wang X. Adsorption of methyl orange dye onto multiwalled carbon nanotubes. Procedia Environ Sci, **18**, 890 (2013). http://doi.org/10.1016/j.proenv.2013.04.120.

[3] Mittal A, Kurup L, Mittal J. Freundlich and Langmuir adsorption isotherms and kinetics for the removal of Tartrazine from aqueous solutions using hen feathers. J Hazard Mater, **146**, 243 (2007). http://doi.org/10.1016/j.jhazmat.2006.12.012.

[4] Pokhrel D, Viraraghavan T. Treatment of pulp and paper mill wastewater: a review. Sci Total Environ, **333**, 37 (2004). http://doi.org/10.1016/j.scitotenv.2004.05.017.

[5] Huo Y, Xie Z, Wang X, Li H, Hoang M, Caruso RA. Methyl orange removal by combined visible-light photocatalysis and membrane distillation. Dyes Pigm, **98**, 106 (2013). http://doi.org/10.1016/j.dyepig.2013.02.009.

[6] Zhou L, Gao C, Xu W. Magnetic dendritic materials for highly efficient adsorption of dyes and drugs. ACS Appl Mater Interfaces, **2**, 1483 (2010). http://doi.org/10.1021/am100114f.

[7] Saharan VK, Badve MP, Pandit AB. Degradation of Reactive Red 120 dye using hydrodynamic cavitation. Chem Eng J, **178**, 100 (2011). http://doi.org/10.1016/j.cej.2011.10.018.

[8] Tian Y, Liu P, Wang X, Lin H. Adsorption of malachite green from aqueous solutions onto ordered mesoporous carbons. Chem Eng J, **171**, 1263 (2011). http://doi.org/10.1016/j.cej.2011.05.040.

[9] O'Neill C, Hawkes FR, Hawkes DL, Lourenço ND, Pinheiro HM, Delée W. Colour in textile effluents–sources, measurement, discharge consents and simulation: a review. J Chem Technol Biotechnol, **74**, 1009 (1999). http://doi.org/10.1002/(sici)1097-4660(199911)74:11<1009::aid-jctb153>3.0.co;2-n.

[10] Choy KKH, Porter JF, Mckay G. Intraparticle diffusion in single and multicomponent acid dye adsorption from wastewater onto carbon. Chem Eng J, **103**, 133 (2004). http://doi.org/10.1016/j.cej.2004.05.012.

[11] Mahmoodian H, Moradi O, Shariatzadeha B, Salehf TA, Tyagi I, Maity A, Asif M, Gupta VK. Enhanced removal of methyl orange from aqueous solutions by poly HEMA–chitosan-MWCNT nanocomposite. J Mol Liq, **202**, 189 (2015). http://doi.org/10.1016/j.molliq.2014.10.040.

[12] Rao AV, Jain BL, Gupta IC. Impact of textile industrial effluents on agricultural land. Indian J Environ Health, **35**, 132 (1993).

[13] Hosseini S, Khan MA, Malekbala MS, Cheah W, Choong TSY. Carbon coated monolith, a mesoporous material for the removal of methyl orange from aqueous phase: adsorption and desorption studies. Chem Eng J, **171**, 1124 (2011). http://doi.org/10.1016/j.cej.2011.05.010.

[14] Robinson T, McMullan G, Marchant R, Nigam P. Remediation of dyes in textile effluent: a critical review on current treatment technologies with a proposed alternative. Bioresour Technol, **77**, 247 (2001). http://doi.org/10.1016/s0960-8524(00)00080-8.

[15] Mohammadi N, Khani H, Gupta VK, Amereh E, Agarwal S. Adsorption process of methyl orange dye onto mesoporous carbon material–kinetic and thermodynamic studies. J Colloid Interface Sci, **362**, 457 (2011). http://doi.org/10.1016/j.jcis.2011.06.067.

[16] Rai HS, Bhattacharyya MS, Singh J, Bansal TK, Vats P, Banerjee UC. Removal of dyes from the effluent of textile and dyestuff manufacturing industry: a review of emerging techniques with reference to biological treatment. Crit Rev Environ Sci Technol, **35**, 219 (2005). http://doi.org/10.1080/10643380590917932.

[17] Xu YY, Zhou M, Geng HJ, Hao HJ, Ou QQ, Qi SD, Chen HL, Chen XG. A simplified method for synthesis of Fe_3O_4@PAA nanoparticles and its application for the removal of basic dyes. Appl Surf Sci, **258**, 3897 (2012). http://doi.org/10.1016/j.apsusc.2011.12.054.

[18] Arshadi M, SalimiVahid F, Salvacion JWL, Soleymanzadeh M. Adsorption studies of methyl orange on an immobilized Mn-nanoparticle: kinetic and thermodynamic. RSC Adv, **4**, 16005 (2014). http://doi.org/10.1039/c3ra47756h.

[19] Zhu HY, Jiang R, Xiao L, Zeng GM. Preparation, characterization, adsorption kinetics and thermodynamics of novel magnetic chitosan enwrapping nanosized γ-Fe_2O_3 and multi-walled carbon nanotubes with enhanced adsorption properties for methyl orange. Bioresour Technol, **101**, 5063 (2010). http://doi.org/10.1016/j.biortech.2010.01.107.

[20] Zhang P, An Q, Guo J, Wang CC. Synthesis of mesoporous mag-

netic Co-NPs/carbon nanocomposites and their adsorption property for methyl orange from aqueous solution. J Colloid Interface Sci, **389**, 10 (2013). http://doi.org/10.1016/j.jcis.2012.08.022.

[21] Cheah W, Hosseini S, Khan MA, Chuah TG, Choong TSA. Acid modified carbon coated monolith for methyl orange adsorption. Chem Eng J, **215**, 747 (2013). http://doi.org/10.1016/j.cej.2012.07.004.

[22] Huang R, Liu Q, Huo J, Yang B. Adsorption of methyl orange onto protonated cross-linked chitosan. Arabian J Chem, Available Online: May 30 (2013). http://doi.org/10.1016/j.arabjc.2013.05.017.

[23] Gu Z, Deng B, Yang J. Synthesis and evaluation of iron-containing ordered mesoporous carbon (FeOMC) for arsenic adsorption. Microporous Mesoporous Mater, **102**, 265 (2007). http://doi.org/10.1016/j.micromeso.2007.01.011.

[24] Nejad NF, Shams E, Amini MK, Bennett JC. Synthesis of magnetic mesoporous carbon and its application for adsorption of dibenzothiophene. Fuel Process Technol, **106**, 376 (2013). http://doi.org/10.1016/j.fuproc.2012.09.002.

[25] Valix M, Cheung WH, McKay G. Roles of the textural and surface chemical properties of activated carbon in the adsorption of acid blue dye. Langmuir, **22**, 4574 (2006). http://doi.org/10.1021/la051711j.

[26] Goscianska J, Olejnik A, Pietrzak R. Comparison of ordered mesoporous materials sorption properties towards amino acids. Adsorption, **19**, 581 (2013). http://doi.org/10.1007/s10450-013-9481-z.

[27] Mittal A, Malviya A, Kaur D, Mittal J, Kurup L. Studies on the adsorption kinetics and isotherms for the removal and recovery of methyl orange from wastewaters using waste materials. J Hazard Mater, **148**, 229 (2007). http://doi.org/10.1016/j.jhazmat.2007.02.028.

[28] Hesas RH, Arami-Niya A, Daud WMAW, Sahu JN. Preparation and characterization of activated carbon from apple waste by microwave-assisted phosphoric acid activation: application in methylene blue adsorption. BioResources, **8**, 2950 (2013). http://doi.org/10.15376/biores.8.2.2950-2966.

[29] Pal J, Deb MK, Deshmukh DK, Verma D. Removal of methyl orange by activated carbon modified by silver nanoparticles. Appl Water Sci, **3**, 367 (2013). http://doi.org/10.1007/s13201-013-0087-0.

[30] Qiu M, Xiong S, Wang G, Xu J, Luo P, Ren S, Wang Z. Kinetic for adsorption of dye methyl orange by the modified activated carbon from rice husk. Adv J Food Sci Technol, **9**, 140 (2015). http://doi.org/10.19026/ajfst.9.1949.

[31] Wu YH, Yu Q, Xu HD, Liu NY, Sun MZ, Zhu J. Adsorption behavior and kinetics of methyl orange in water on activated carbon. Adv Mater Res, **549**, 318 (2012). http://doi.org/10.4028/www.scientific.net/amr.549.318

[32] Sarici-Ozdemir C. Adsorption and desorption kinetics behaviour of methylene blue onto activated carbon. Physicochem Probl Miner Process, **48**, 441 (2012). http://dx.doi.org/10.5277/ppmp120210.

[33] Fang J, Wang X, Lin T. Functional Applications of Electrospun Nanofibers. In: Lin T, ed. Nanofibers: Production, Properties and Functional Applications, Intec-Open Access Publisher, Rijeka, 287 (2011). http://doi.org/10.5772/24998

[34] Zak AK, Majid WHA, Abrishami ME, Yousefi R. X-ray analysis of ZnO nanoparticles by Williamson–Hall and size–strain plot methods. Solid State Sci, **13**, 251 (2011). http://doi.org/10.1016/j.solidstatesciences.2010.11.024.

[35] Monash P, Pugazhenthi G. Adsorption of crystal violet dye from aqueous solution using mesoporous materials synthesized at room temperature. Adsorption, **15**, 390 (2009). http://doi.org/10.1007/s10450-009-9156-y.

[36] Bidhendi ME, Bidhendi GRN, Mehrdadi N, Rashedi H. Modified mesoporous silica (SBA–15) with trithiane as a new effective adsorbent for mercury ions removal from aqueous environment. J Environ Health Sci Eng, **12**, 1 (2014). http://doi.org/10.1186/2052-336x-12-100.

[37] Das B, Mondal NK, Roy P, Chattaraj S. Equilibrium, kinetic and thermodynamic study on chromium (VI) removal from aqueous solution using Pistia stratiotes biomass. Chem Sci Trans, **2**, 85 (2013). http://doi.org/10.7598/cst2013.318.

[38] Deng H, Zhang G, Xu X, Tao G, Dai J. Optimization of preparation of activated carbon from cotton stalk by microwave assisted phosphoric acid-chemical activation. J Hazard Mater, **182**, 217 (2010). http://doi.org/10.1016/j.jhazmat.2010.06.018.

[39] Lahaye J, Ehrburger P. Fundamental Issues in Control of Carbon Gasification Reactivity (Vol. 192), Springer Science & Business Media, New York (1991). http://doi.org/10.1007/978-94-011-3310-4.

[40] Rouquerol J, Rouquerol F, Llewellyn PL, Maurin G, Sing KSW. Adsorption by Powders and Porous Solids: Principles, Methodology and Applications, Academic Press, Amsterdam (2013).

[41] Guo L, Li G, Liu J, Meng Y, Tang Y. Adsorptive decolorization of methylene blue by crosslinked porous starch. Carbohydr Polym, **93**, 374 (2013). http://doi.org/10.1016/j.carbpol.2012.12.019.

[42] Qu D. Studies of the activated carbons used in double-layer supercapacitors. J Power Sources, **109**, 403 (2002). http://doi.org/10.1016/s0378-7753(02)00108-8.

[43] Choi JS, Kim TH, Choo KY, Sung JS, Saidutta MB, Ryu SO, Song SD, Ramachandra B, Rhee YW. Direct synthesis of phenol from benzene on iron-impregnated activated carbon catalysts. Appl Catal A Gen, **290**, 1 (2005). http://doi.org/10.1016/j.apcata.2005.04.060.

[44] Deng H, Li G, Yang H, Tang J, Tang J. Preparation of activated carbons from cotton stalk by microwave assisted KOH and K_2CO_3 activation. Chem Eng J, **163**, 373 (2010). http://doi.org/10.1016/j.cej.2010.08.019.

[45] Li X, Zuo Y, Zhang Y, Fu Y, Guo Q. In situ preparation of K_2CO_3 supported Kraft lignin activated carbon as solid base catalyst for biodiesel production. Fuel, **113**, 435 (2013). http://doi.org/10.1016/j.fuel.2013.06.008.

[46] Yang T, Lua AC. Textural and chemical properties of zinc chloride activated carbons prepared from pistachio-nut shells. Mater Chem Phys, **100**, 438 (2006). http://doi.org/10.1016/j.matchemphys.2006.01.039.

[47] Liu Y, Watanasiri S. Representation of liquid-liquid equilibrium of mixed-solvent electrolyte systems using the extended electrolyte NRTL model. Fluid Phase Equilib, **116**, 193 (1996). ttps://doi.org/10.1016/0378-3812(95)02887-0.

[48] Fengel D. Characterization of cellulose by deconvoluting the OH valency range in FTIR spectra. Holzforschung, **46**, 283 (1992). http://doi.org/10.1515/hfsg.1992.46.4.283.

[49] Zawadzki J. Infrared-spectroscopy in surface-chemistry of carbons. Chem Phys Carbon, **21**, 147 (1989).

[50] Fanning PE, Vannice MA. A DRIFTS study of the formation of surface groups on carbon by oxidation. Carbon, **31**, 721 (1993). http://doi.org/10.1016/0008-6223(93)90009-y.

[51] Puziy AM, Poddubnaya OI, Martínez-Alonso A, Suárez-García F, Tascón JMD. Synthetic carbons activated with phosphoric acid: I. surface chemistry and ion binding properties. Carbon, **40**, 1493

(2002). http://doi.org/10.1016/s0008-6223(01)00317-7.

[52] Ivanova BB, Arnaudov MG, Bontchev PR. Linear-dichroic infrared spectral analysis of Cu(I)–homocysteine complex. Spectrochim Acta A Mol Biomol Spectrosc, **60**, 855 (2004). http://doi.org/10.1016/s1386-1425(03)00310-x.

[53] Zahoor A, Christy M, Hwang YJ, Lim YR, Kim P, Nahm KS. Improved electrocatalytic activity of carbon materials by nitrogen doping. Appl Catal B Environ, **147**, 633 (2014). http://doi.org/10.1016/j.apcatb.2013.09.043.

[54] Abbas M, Kaddour S, Trari M. Kinetic and equilibrium studies of cobalt adsorption on apricot stone activated carbon. J Ind Eng Chem, **20**, 745 (2014). http://doi.org/10.1016/j.jiec.2013.06.030.

[55] Shin S, Jang J, Yoon SH, Mochida I. A study on the effect of heat treatment on functional groups of pitch based activated carbon fiber using FTIR. Carbon, **35**, 1739 (1997). http://doi.org/10.1016/s0008-6223(97)00132-2.

[56] Meldrum BJ, Rochester CH. In situ infrared study of the modification of the surface of activated carbon by ammonia, water and hydrogen. J Chem Soc Faraday Trans, **86**, 1881 (1990). http://doi.org/10.1039/ft9908601881.

[57] Terzyk AP. The influence of activated carbon surface chemical composition on the adsorption of acetaminophen (paracetamol) in vitro: Part II. TG, FTIR, and XPS analysis of carbons and the temperature dependence of adsorption kinetics at the neutral pH. Colloids Surf A Physicochem Eng Asp, **177**, 23 (2001). http://doi.org/10.1016/s0927-7757(00)00594-x.

[58] Guo J, Lua AC. Textural and chemical properties of adsorbent prepared from palm shell by phosphoric acid activation. Mater Chem Phys, **80**, 114 (2003). http://doi.org/10.1016/s0254-0584(02)00383-8.

[59] Lua AC, Yang T. Effect of activation temperature on the textural and chemical properties of potassium hydroxide activated carbon prepared from pistachio-nut shell. J Colloid Interface Sci, **274**, 594 (2004). http://doi.org/10.1016/j.jcis.2003.10.001.

[60] An D, Guo Y, Zou B, Zhu Y, Wang Z. A study on the consecutive preparation of silica powders and active carbon from rice husk ash. Biomass Bioenergy, **35**, 1227 (2001). http://doi.org/10.1016/j.biombioe.2010.12.014.

[61] Jung MW, Ahn KH, Lee Y, Kim KP, Rhee JS, Park JT, Paeng KJ. Adsorption characteristics of phenol and chlorophenols on granular activated carbons (GAC). Microchem J, **70**, 123 (2001). http://doi.org/10.1016/s0026-265x(01)00109-6.

[62] Lagergren S. About the theory of so-called adsorption of soluble substances. Kungliga Svenska Vetenskapsakademiens Handlingar, **24**, 1 (1898).

[63] Ho YS, McKay G. The kinetics of sorption of divalent metal ions onto sphagnum moss peat. Water Res, **34**, 735 (2000). http://doi.org/10.1016/s0043-1354(99)00232-8.

[64] Weber WJ, Morris JC. Kinetics of adsorption on carbon from solution. J Sanit Eng Div, **89**, 31 (1963).

[65] Blanchard G, Maunaye M, Martin G. Removal of heavy metals from waters by means of natural zeolites. Water Res, **18**, 1501 (1984). http://doi.org/10.1016/0043-1354(84)90124-6.